FIBRES & TEXTILES in Eastern Europe

sciendo

FIBRES & TEXTILES in Eastern Europe

Research Article • DOI: 10.2478/ftee-2023-0050 FTEE • 31(5) • 2023 • 99–108

Evaluation of Insulation against Contact Heat, Radiant Heat and Sensory Comfort of Basalt Fabric-Based Composites with Parylene C Coating

Magdalena Tokarska[1]*, Pamela Miśkiewicz[1],
Adam K. Puszkarz[2], Andrzej Nosal[3]

[1] *Lodz University of Technology, Faculty of Material Technologies and Textile Design, Institute of Architecture of Textiles, 116 Zeromskiego St., 90-543 Lodz, Poland*
[2] *Lodz University of Technology, Faculty of Material Technologies and Textile Design, Institute of Material Science of Textiles and Polymer Composites, 116 Zeromskiego St., 90-543 Lodz, Poland*
[3] *Lodz University of Technology, Faculty of Mechanical Engineering, Institute of Materials Science and Engineering, 1/15 Stefanowskiego St., 90-924 Lodz, Poland*
* *Corresponding author. E-mail: magdalena.tokarska@p.lodz.pl*

Abstract
The article concerns research on using Parylene C coating on basalt fabric-based composites with potential use in protective clothing to improve their insulation against contact heat and radiant heat, as well as the sensory comfort of the user. The outcomes of the contact heat method showed that applying Parylene C coating improved the thermal insulation of all tested composites. Two of them achieved the first efficiency level of protection. The results of the radiant heat method presented that using the Parylene C coating did not cause changes in the thermal insulation against heat radiation of all tested materials; the radiant heat transfer index reached values in the range of 12.4 - 12.9 s. X-ray tomography (micro-CT) allowed for identifying breaks/snaps in basalt fibers irritating the user's skin in direct contact with the composite. Micro-CT results also showed that using Parylene C coating eliminated the effect of skin irritation and increased the usability of basalt fabrics in clothing.

Keywords
basalt fabric, Parylene C, thermal protection, micro-CT, colorimetry.

1. Introduction

Basalt is a fine-grained extrusive igneous rock that arose as a result of the rapid cooling of low-viscosity lava rich in magnesium and iron [1,2]. Basalt has a relatively homogeneous chemical structure and, hence, the ability to form fibers in a molten state. Basalt fibers' chemical composition was determined [3] and quantitatively is as follows (in %wt.): 51.6–59.3 SiO_2, 14.6–18.3 Al_2O_3, 5.9–9.4 CaO, 3.0–5.3 MgO, 9.0–14.0 FeO + Fe_2O_3, 0.8–2.3 TiO_2, 0.8–2.3 Na_2O + K_2O, and 0.09–0.13, among others. Basalt is non-toxic and does not contain any toxic impurities or heavy metals. Therefore, it has many potential applications [4]. Basalt is an alternative raw material for the production of textile materials. Basalt materials have good mechanical properties [5-7]. They are characterized by good thermal properties (low thermal conductivity, good thermal resistance) and low moisture absorption [1,6,8,9]. In addition, basalt fabrics are non-flammable and can be used in the temperature range -260÷800 °C. They are resistant to UV radiation, corrosion, and the action of microorganisms, and also do not emit toxic substances in reaction with water or air.

Basalt fabrics are exceptional materials that fit into a new range of composite materials and products. A particular area of application is protective equipment [10-16]. Protective clothing is an effective barrier between the human body and the environment [17,18]. Basalt fabric poses no risk to human beings but is unsuitable for direct use. Breaks into long thin pieces occur during handling in the fabric [9,19]. Basalt fibers can cause redness and irritation through splinters of filament entering the skin or other body areas, eyes, and the respiratory tract. Basalt yarns are slippery. It is recommended to tape the cut line to keep it from fraying. The magnetron sputtering method is often used for surface modification of basalt fabrics with metals and ceramics [20,21]. One-side modification enables to improve the thermal properties of the composites from the point of view of use as a protective material. Moreover, the coating improves basalt fiber adhesion in the fabric. Basalt fabrics can also be used as a layer of multi-layer packaging protecting the user in a hot work environment [22-24]. It was noticed that composites with a modified outer layer reached a certain level of protection against contact and radiant heat [24].

Parylene (poly-para-xylylene-based polymer) is a crystal-clear, polycrystalline, and amorphous linear polymer discovered by Szwarc [25] in 1947. Gorham [26] patented the parylene coating process in 1967. Parylene is formed from granular powdered material called dimer (di-para-xylylene). Dimer is converted under heat and a vacuum to a gaseous polymerizing monomer suitable for deposition on substrates at room temperature [27-30]. The poly-para-xylylene-based polymer can be used with metals and plastics as a coating for electrical components and assemblies. This polymer has low surface friction. It also has excellent chemical and dielectric barrier properties. Parylene hardly absorbs any water and is resistant to water diffusion. It shows

high corrosion resistance. The most widely used parylenes are Parylene N, C, and D [29]. Parylene N has the best crevice-penetration capability, the best dielectric strength, the lowest coefficient of friction, the lowest elongation, and the lowest dissipation factor. However, there is a problem connected with preventing film deposition in areas that are to remain uncoated. Comparing Parylene N and C, the second one has more thermal stability and chemical and moisture resistance. Parylene C is the best moisture barrier of all the parylenes mentioned. It can be deposited relatively quickly on the sample surface, with reasonable thickness control. The dielectric strength of Parylene C is slightly less than that of Parylene N, as is its crevice-penetration ability. Parylene D has the lowest crevice-penetration ability of the parylenes described. The parylene forms the hardest coating and undergoes the least elongation. The polymer shows the greatest temperature stability. Parylene C and Parylene N have medical applications as a coating. Parylene D is more suited to industrial applications where basic requirements are physical toughness, chemical resistance, and thermal stability. Parylene coating is very thin, transparent, smooth, chemically inert, and has dielectric properties. Parylene can perfectly conform to the substrate because it has good adhesion [31]. Parylene coatings provide maximum barrier protection due to their lightweight. This polymer can form protective and insulating coatings on electronic devices and generate extremely thin, pinhole-free films [32,33]. Parylene C is widely used in medicine, for example, to implant covering [34] or as an encapsulation material for implanted neural prostheses [35]. Parylene C shows high biocompatibility, biostability, and the possibility of producing a thin, continuous, and inert coating [36]. In general, Parylene C is a versatile supporting material suitable for application in flexible materials. Parylene coating reproduces the surface texture of substrate material very well [37]. The poly-para-xylylene-based polymer has very low thermal conductivity [38]. The thermal conductivity of parylene coating is dependent on the coating thickness, as was shown for Parylene C [39]. Parylene C is also used as a coating of silk fabric to protect it against exposure to daylight and ultraviolet light, which cause the aging of the material [40]. Parylene coating makes silk fabrics somewhat stiffer and smoother.

It was noticed that the modified basalt fabrics used separately or in a multi-layer textile composite are a promising solution from the point of view of the user's thermal comfort in a hot environment. However, the inner layer in the composites was unmodified basalt fabric in direct contact with the skin. Due to the irritating influence of basalt fabric, it was found that fabric with the basalt composite should be modified. To provide user comfort, the skin contact side of basalt fabric must be coated. Parylene C coating was used due to its high biocompatibility, as well as its conformity, penetration, and purity. The advantages result from the diffusion mechanism of adding monomers to the surface of the coating, which eliminates the presence of the liquid phase and the related problems caused by surface tension in wet methods. Also, the process in the so-called "vacuum" makes it possible to thoroughly clean the surface of the adsorbed moisture of gases just before the process, which makes the applied coating even better adhere to the coated elements.

The main aim of the research work is to improve the properties of basalt fabrics from the user's comfort point of view and obtain a skin-friendly material that can be used as an inner layer in the multi-layer textile composite in direct contact with human skin.

2. Materials

Fabrics made of basalt fibers were selected for tests. The basic parameters of the basalt fabrics are given in Table 1.

Optical microscopy images of tested woven fabrics using the optical microscope Delta Optical Smart 5MP PRO (Delta Optical, Warsaw, Poland) and the software Delta Optical Smart Analysis Pro 1.0.0 are shown in Figure 1.

The breaks into long thin yarns during handling in basalt fabric are shown in Figure 2. As a result of breaks and snaps of fibers, protruding parts appear and irritate the user's skin.

Basalt fabrics as the inner layer in the multi-layer textile composite and in direct contact with the skin were modified.

3. Methods

3.1. Parylene C coating technology

The SCS Labcoater™ 2 Parylene Deposition System (PDS 2010) (Speciality Coating Systems, Indianapolis, USA) was used for the application of Parylene C coating. To apply the Parylene C coating, a basalt fabric sample was clamped in a holder placed on a turntable

Sample	Weave	Linear mass of warp/weft, tex	Warp density, threads·cm^{-1}	Weft density, threads·cm^{-1}	Thickness, mm	Areal density, g·m^{-2}	Bulk density, kg·m^{-3}
B1	Plain	138	11	9	0.480 (4%)	284 (6%)	592
B2	Plain	293	9	8	0.552 (5%)	391 (7%)	711
B3	Plain	189	11	9	0.582 (3%)	430 (8%)	741
B4	Twill	296	9	6	0.802 (4%)	731 (5%)	914

Table 1. Basalt fabric parameters (mean value with a variation coefficient)

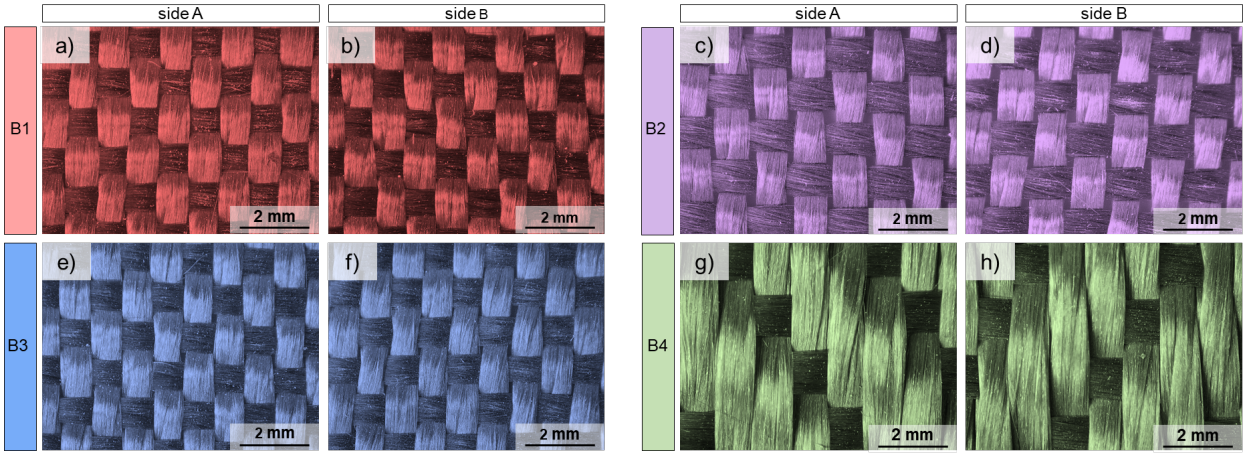

Fig. 1. Optical microscopy images of both sides of basalt fabrics

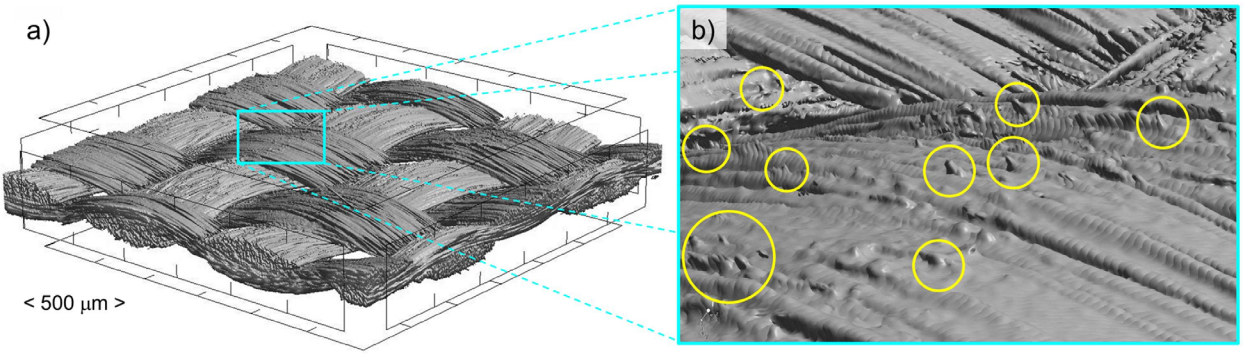

Fig. 2. Micro-CT images of damaged surface: a) yarns of basalt fabric B1 (surface area: 3 mm × 3 mm), b) an enlarged area of the fabric inside the rectangle illustrating protruding parts of basalt fibers (inside yellow circles)

in the reactor chamber. Next, 8 g of parylene dimer was weighed in a suitably profiled, disposable aluminum foil boat, and placed in a sublimation apparatus. An amount of 8 g of dimer corresponds to 5 μm of coating. After closing the reactor chamber and the sublimation apparatus, the system was pumped down and left for a day. Next, to protect the vacuum pumps of the system from monomer particles, 10 minutes before turning on the pyrolizer furnace heating, a cold trapping operation was performed using a liquid nitrogen cold trap. Then, the initial process pressure PLA1 was set to 7 units and the process pressure SP to 10 units. When the pyrolizer reached the set pressure SP, the controller turned on the heating of the sublimation apparatus and controlled the temperature using the PID controller. The temperature control was carried out in such a way that the pressure in the chamber was maintained at the set level of 10 units, guaranteeing a constant rate of deposition. The process was completed when the entire dimer evaporated, as evidenced by the increase in the temperature of the sublimator with a simultaneous decrease in the pressure in the chamber to the value of 7 units. After the pyrolizer furnace cooled down, the system was vented and the sample with the Parylene C coating applied was removed from the chamber reactor. As a result of Parylene C coating, double-sided modified basalt fabrics (composites) were obtained: BP1, BP2, BP3, and BP4 corresponding to the unmodified fabrics B1, B2, B3, and B4, respectively. The method of changing the characteristics of a textile material as a result of Parylene C coating was patented [41].

3.2. Protective thermal properties

In the framework of protective thermal properties of modified basalt fabrics, resistances to contact and radiant heat were selected. Standard ISO 12127-1:2016 [42] was used as recommended to determine the contact heat resistance of the basalt fabrics and composites. A test sample with a diameter of 8 cm was placed on a calorimeter and then put into contact with a heater heated to a chosen temperature of 250°C according to the ISO 11612:2015-11 standard [43]. The standard specifies performance requirements for clothing to protect the wearer's body, except the hands. The threshold time t_t, expressed in seconds, was measured from the moment the sample contacted the heater until the calorimeter temperature rose by 10°C. The scheme of the measurement system according to ISO 12127-1:2016 is shown in Figure 3. Three efficiency levels were taken into account [43] F1 when $t_t \in [5.0,10.0)$ s, F2 when $t_t \in [10.0,15.0)$ s, and F3 for $t_t \geq 15.0$ s.

Standard ISO 6942:2022 [44] was used as recommended to determine the radiant

heat resistance of the basalt fabrics and composites (a scheme of the measurement system is presented in Figure 4). The tests described were carried out on representative single or multi-layer textiles or other materials intended for clothing for protection against heat. A rectangular sample with dimensions of 8×17 cm placed on an appropriate holder was subjected to thermal radiation for a set time. An incident heat flux density of 20 kW/m^2 was assumed. The time, expressed in seconds, to achieve a calorimeter temperature rise of 24.0±0.2°C when tested according to method B was measured.

The radiant heat transfer index $RHTI_{24}$ (time to achieve a temperature rise of 24°C in the calorimeter when testing a sample with a specified incident heat flux density) (this temperature rise indicates that the user experienced second-degree burns)) was calculated from the mean value of the time. Four efficiency levels were taken into account [43] C1 when $RHTI_{24}$ Î [7.0,20.0) s, C2 when $RHTI_{24}$ ϵ [20.0,50.0) s, C3 when $RHTI_{24}$ ϵ [50.0,95.0) s, and C4 for $RHTI_{24} \geq 95.0$ s.

3.3. X-ray microtomography

Structural parameters and 3D reconstruction of the modified woven fabrics were determined using X-ray micro-computed tomography (SkyScan 1272; Bruker, Kontich, Belgium). Micro-CT outcomes were obtained by applying the following scanning conditions: X-ray source voltage 60 kV, X-ray source current 166 µA, and pixel size 5.5 µm. A 180° rotation was performed with a rotation step of 0.2°, and an Al 0.25 mm filter was selected. Square samples with dimensions of 3×3 mm) were considered. Micro-CT is based on the absorption of X-rays by the tested material and allows characterization of the internal structure of objects on a microscale [45]. When the tested material consists of phases with different absorption of X-ray radiation (e.g., basalt, parylene, or air), it is possible to identify these phases, determine their shape, volume, surface, and spatial orientation inside the material, and thus calculate the porosity. In such a way, in the research presented, it was possible to determine the porosity of the woven fabrics (air content in the woven fabric) and the content of deposited material (Parylene C).

3.4. Colorimetry analysis

Surface color parameters of textile materials can change with their different processing [46]. The basalt fabric surface modified with a parylene coating was subjected to colorimetry analysis to assess the effect of modification on the resistance of the composite to radiant heat. A square area with sides of 2 cm was separated for study from a rectangular sample with dimensions of 8×17 cm. Color measurement is based on experimental observations according to the International Commission on Illumination (CIE) color specification system [47]. The CIE standard defines procedures for calculating the coordinates of a CIELAB color space. A DigiEye System (VeriVide, Leicester, UK) was used to assess the basalt fabric-modified surface. The system enables non-contact digital color imaging. CIE illuminant D65 was assumed and defined as a representation of natural daylight considered as an equivalent light source from a tungsten filament (as a radiator) when heated at 65040 K. The CIE color difference formula (CIE ΔE_{2000}) was employed in this system, described in detail in [48,49].

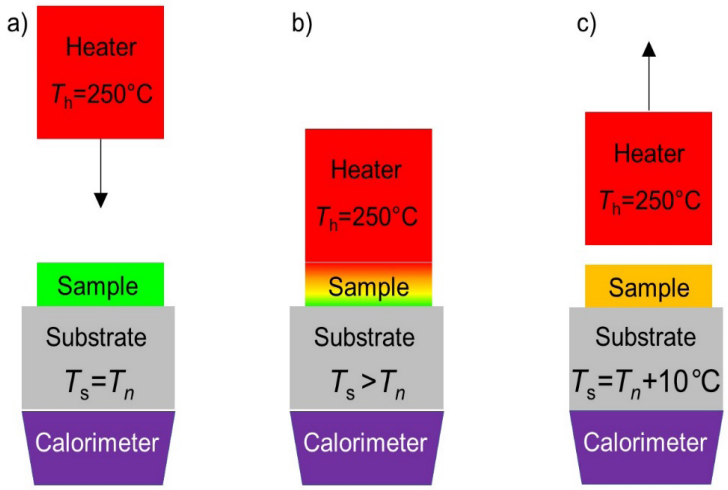

Fig. 3. Scheme of the measurement system according to ISO 12127-1:2016

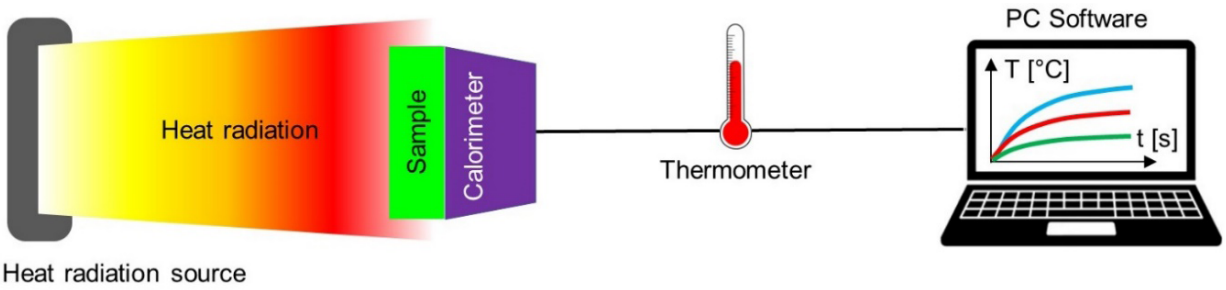

Fig. 4. Scheme of the measurement system according to EN ISO 6942:2022

Let a pair of color values in the CIELAB color space be represented by coordinates (L_1*,a_1*,b_1*) and (L_2*,a_2*,b_2*). The CIEDE2000 color difference between them is designated as follows:

$$\Delta E_{2000}(L_1^*,a_1^*,b_1^*;L_2^*,a_2^*,b_2^*)=\Delta E_{00}, \quad (1)$$

where L* is the brightness-darkness component (the percentage of chromatic colors), a* the green-red component with the green in the negative direction and the red in the positive direction (value of parameter a* in the range of -100 to 100), and b* is the blue-yellow component with the blue in the negative direction and the yellow in the positive direction (value of parameter b* is in the range of -100 to 100). Parameters L*, a*, and b* combine Cartesian coordinates and form a 3D color space in the cylindrical coordinate system.

Geometrical parameter	Composite			
	BP1	BP2	BP3	BP4
Total porosity, %	41.86	46.62	60.29	47.89
Yarn porosity (weft), %	35.61	32.91	30.34	39.57
Yarn porosity (warp), %	22.61	31.14	31.25	35.41
Weft density, cm^{-1}	9.3	8.4	8.9	6.6
Warp density, cm^{-1}	11.4	9.2	11.3	9.6
Density of yarns, cm^{-2}	106	77	101	63
Major axis of elliptic yarn cross-section (weft), a_{we}, mm	0.767	0.771	0.644	1.089
Minor axis of elliptic yarn cross-section (weft), b_{we}, mm	0.177	0.156	0.235	0.295
Weft flattering coefficient, $e_{we} = b_{we} \cdot a_{we}^{-1}$	0.231	0.202	0.365	0.271
Major axis of elliptic yarn cross-section (warp), a_{wa}, mm	0.838	0.855	0.820	1.168
Minor axis of elliptic yarn cross-section (warp), b_{wa}, mm	0.134	0.311	0.174	0.306
Warp flattering coefficient, $e_{wa} = b_{wa} \cdot a_{wa}^{-1}$	0.160	0.364	0.212	0.262

Table 2. Structural parameters of composites determined using micro-CT

The value of ΔE_{00} is measured on a scale from 0 to 100. Standard perception ranges are as follows [49]:

- $0 < \Delta E_{00} < 1$ – a normally invisible difference, an observer does not notice the difference,
- $1 \leq \Delta E_{00} < 2$ – a very small difference, only an experienced observer notices the difference,
- $2 \leq \Delta E_{00} < 3.5$ – a medium difference, an inexperienced observer also notices the difference,
- $3.5 \leq \Delta E_{00} < 5$ – an obvious difference, an observer notices a clear color difference,
- $5 \leq \Delta E_{00}$ – a very obvious difference, an observer notices two different colors.

3.5. Uncertainty analysis

The rules for evaluating measurement uncertainty are described in the document [50]. A measure of uncertainty is the expanded uncertainty given by the formula:

$$U = k_p u_c(y), \quad (2)$$

where k_p is the coverage factor, and $u_C(y)$ is the combined standard uncertainty of y (measurand).

The expanded uncertainty is an interval $[y–U, y+U]$ about the measurement result that may be expected to encompass a large fraction of the distribution of values that could reasonably be attributed to the measurand. An coverage factor k_p equal to 2 is assumed, which means that the quoted uncertainty defines an interval having a 95% level of confidence.

The combined standard uncertainty of y is as follows:

$$u_C^2(y) = \sum_{i=1}^{N} \left[\left(\frac{\partial f}{\partial x_i} \right)^2 (u_A^2(x_i) + u_B^2(x_i)) \right] \quad (3)$$

where $u_A(x_i)$ is Type A standard uncertainty, $u_B(x_i)$ Type B standard uncertainty, f the functional relationship between y and input quantities x_i on which y depends, and $\frac{\partial f}{\partial x_i}$ is the sensitivity coefficient.

Type A standard uncertainty estimated from n_i independent repeated observations x_i is given by:

$$u_A(x_i) = \sqrt{\frac{\sum_{i=1}^{n_i}(x_{ik} - \bar{x}_i)^2}{n_i(n_i - 1)}} \quad (4)$$

where $\bar{x}_i$ is the estimate of input quantity x_i.

Type B standard uncertainty is determined based on available information on the possible variability of the input quantity. Assuming a rectangular distribution of possible values, Type B uncertainty can be expressed as:

$$u_B(x_i) = \frac{d_e}{\sqrt{3}} \quad (5)$$

where d_e is the resolution of the measuring instrument.

4. Results and discussion

Using X-ray micro-computed tomography, morphometric analysis of the modified basalt fabrics (composites BP1, BP2, BP3, BP4) was conducted. The results obtained are given in Table 2. Additionally, weft and warp flattering coefficients and the density of yarns were calculated and juxtaposed in Table 2.

A 3D reconstruction of the composites is shown in Figure 5.

Research results of the resistance to contact heat and radiant heat of the unmodified basalt fabrics and modified fabrics (composites) are presented in Tables 3 and 4, respectively. Measurements were repeated three times, and mean values of parameters t_t and $RHTI_{24}$ were calculated. Additionally, the expanded uncertainty was obtained, assuming $k_p = 2$ (Eq. 2).

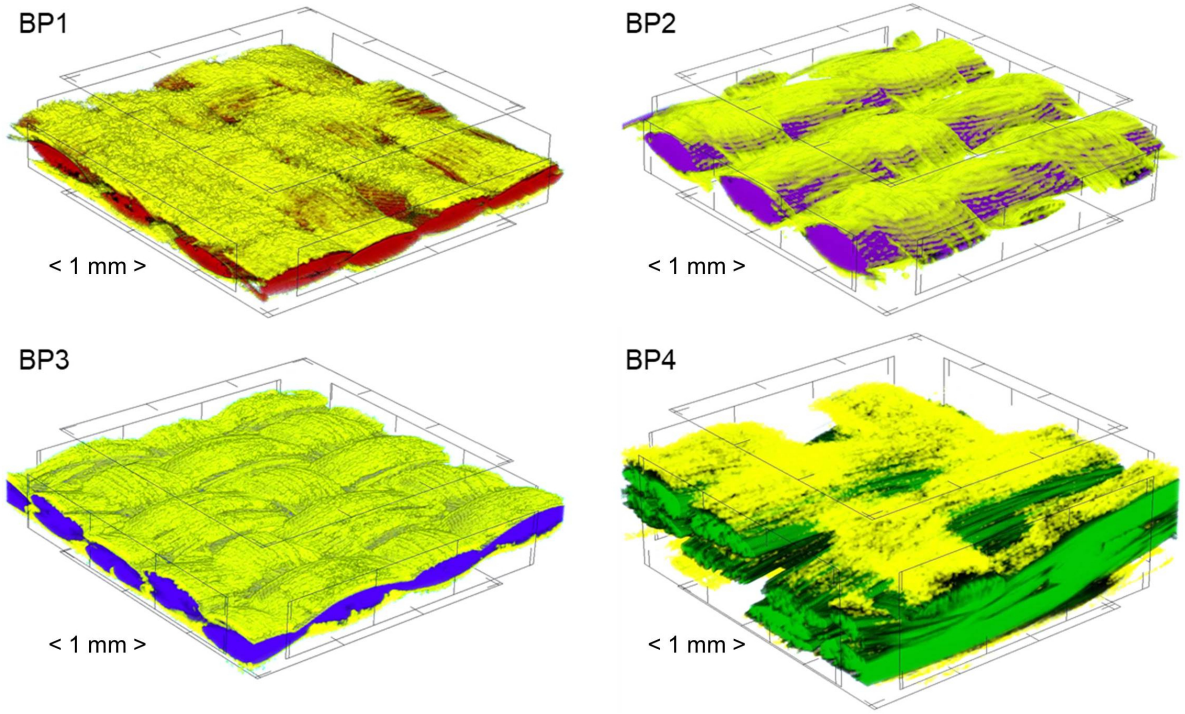

Fig. 5. 3D micro-CT reconstruction of four basalt fabrics with a deposited coating of Parylene C, marked in yellow (all textile surfaces were reduced to dimensions 3×3 mm)

Sample		t_t, s *	Efficiency level	Sample		t_t, s *	Efficiency level
1	B1	3.9 (0.3)	-	5	BP1	4.5 (0.2)	-
2	B2	4.3 (0.8)	-/F1	6	BP2	4.7 (0.2)	-
3	B3	4.4 (0.3)	-	7	BP3	6.7 (1.1)	F1
4	B4	4.5 (0.5)	-	8	BP4	9.7 (0.6)	F1

* *mean value with expanded uncertainty at a 95% level of confidence*

Table 3. Threshold time for basalt fabrics and composites

As shown in Table 3, none of the samples reached the efficiency level in the case of all the unmodified basalt fabrics B1, B2, B3, B4, and two composites BP1 and BP2. The first efficiency level (F1) of protection against contact heat was obtained for composites BP3 and BP4. As shown in Table 4, all the samples reached the first efficiency level (C1) of protection against radiant heat.

Uncertainty analysis was conducted to assess differences between unmodified and modified basalt fabrics. Intervals $[y–U, y+U]$ covering the values of the measurands at a 95% confidence level, i.e. the threshold time and radiant heat transfer index, are shown in Figures 6 and 7, respectively. The interval for each sample is presented separately for better visibility of the results.

The lower and upper ends of the first efficiency level, F1min, and F1max, for the resistance to contact heat are shown in Figure 6. The uncertainty intervals of threshold times partially and also totally overlapped were obtained for all unmodified basalt fabrics (B1, B2, B3, B4) and two modified fabrics BP1, and BP2. Thus, it was found that there are no significant differences between the threshold time values. Moreover, the samples showed no satisfactory resistance to contact heat. The interval obtained for fabric B2 partially coincides with that of threshold time values required for the first efficiency level of protection against contact heat. It was found to be insufficient. Thus, sample B2 showed no resistance to contact heat. Similar to the case of B2, it was found that composite BP4 did not reach the second efficiency level of protection.

Significant differences between threshold times were observed for the remaining composites BP3 and PB4. The composites reached the first efficiency level of protection. Composite BP3 is thinner than BP4. Composite BP3 is characterized by a high total porosity, exceeding 60% (Table 2). Air generally is an excellent thermal insulator, but it can transmit heat through convection. The air-filled pores inside the fabric are typically separated from each other. The heat flow from one pore to another is not easy. In the case of composite BP4, the total porosity is 48% (Table 2). The composite is the thickest and shows the best resistance to contact heat among the tested samples.

The lower and upper ends of the first efficiency level, C1min, and C1max, for

Sample		$RHTI_{24}$, s *	Efficiency level	Sample		$RHTI_{24}$, s *	Efficiency level
1	B1	12.6 (0.3)	C1	5	BP1	12.4 (0.4)	C1
2	B2	12.6 (0.3)	C1	6	BP2	12.9 (0.4)	C1
3	B3	12.4 (0.3)	C1	7	BP3	12.8 (0.4)	C1
4	B4	12.9 (0.3)	C1	8	BP4	12.8 (0.9)	C1

* *mean value with expanded uncertainty at a 95% level of confidence*

Table 4. Radiant heat transfer index for basalt fabrics and composites

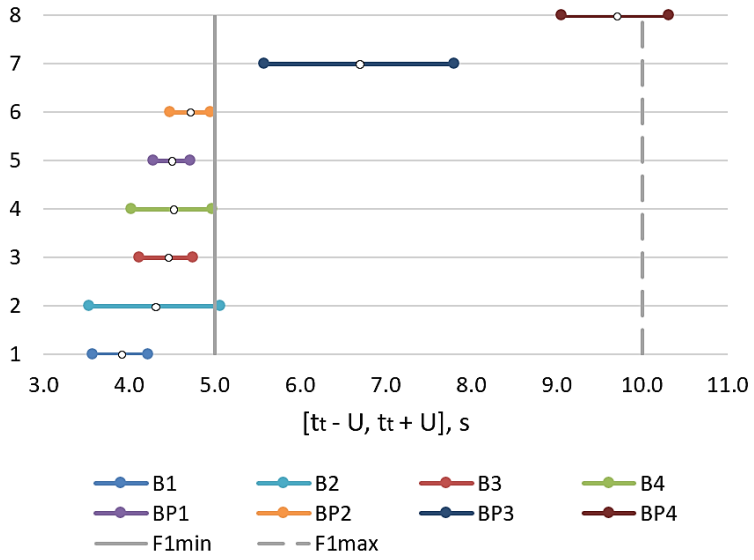

Fig. 6. Uncertainty intervals covering the threshold time for unmodified basalt fabrics and composites

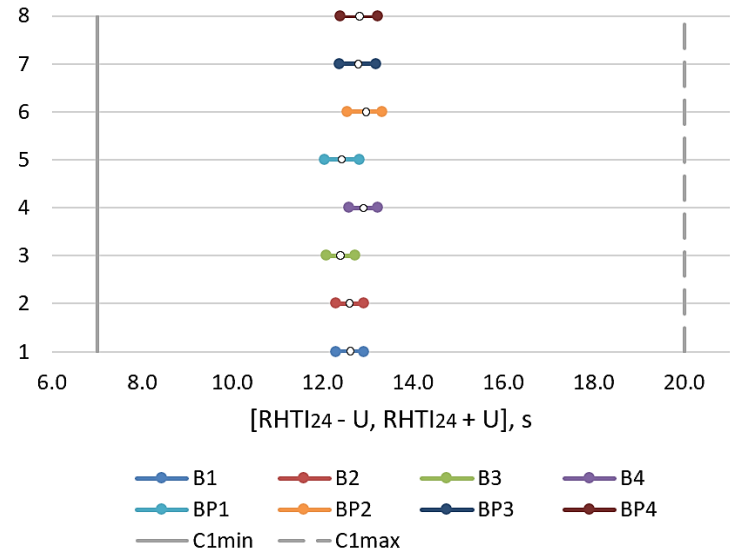

Fig. 7. Uncertainty intervals covering the radiant heat transfer index for unmodified basalt fabrics and composites

the resistance to radiant heat, are shown in Figure 7. The uncertainty intervals of the radiant heat transfer index, obtained for all basalt fabrics and composites, partially overlap or fully overlap. Thus, it was found that there are no significant differences between the radiant heat transfer index values.

Color measurements were conducted to assess the surfaces of the modified basalt fabrics. The color difference between the unmodified and modified basalt fabrics was measured. Measurement results are presented in Table 5.

The value of ΔE_{00} is in the range [1,2), which means that there is a very small difference between the samples' surface colors. Perception of color difference is slight. Thus, it can be considered that the colors of the sample pairs do not differ significantly.

Additionally, a remission measurement of the basalt fabrics and composites was conducted in the spectrum of 400-700 nm. The spectral remission factor R was in the range [10,24]% for all the samples. An example remission curve obtained for BP1 is shown in Figure 8.

The low stream of reflected light from the tested surface confirmed the low-efficiency level of the protection sample against radiant heat. It means that the basalt fabric modified with Parylene C coating should be an inner layer, not an outer layer of a multi-layer textile composite protecting the user in a hot work environment.

Analysis of the effect of the porosity and thickness of the unmodified and modified basalt fabrics on parameters t_t and $RHTI_{24}$ was carried out. The results are shown in Figure 9. It was found that all fabrics (unmodified and modified) were characterized by a comparable value of the $RHTI_{24}$ parameter (the maximum difference is 4% between B4 and BP1). There was also no dependence of the $RHTI_{24}$ parameter on the thickness of the fabrics and their porosity. In the case of unmodified and modified fabrics, an increasing dependence of the t_t parameter

Sample	L_1*	a_1*	b_1*	Sample	L_1*	a_1*	b_1*	ΔE_{00}
B1	51.02	3.76	8.96	BP1	52.06	3.20	9.19	1.67
B2	47.42	2.94	8.53	BP2	47.81	3.02	8.17	1.67
B3	51.27	3.12	9.37	BP3	50.89	3.17	8.75	1.67
B4	48.18	2.97	8.76	BP4	49.72	3.08	8.80	1.67

Table 5. Color measurements results

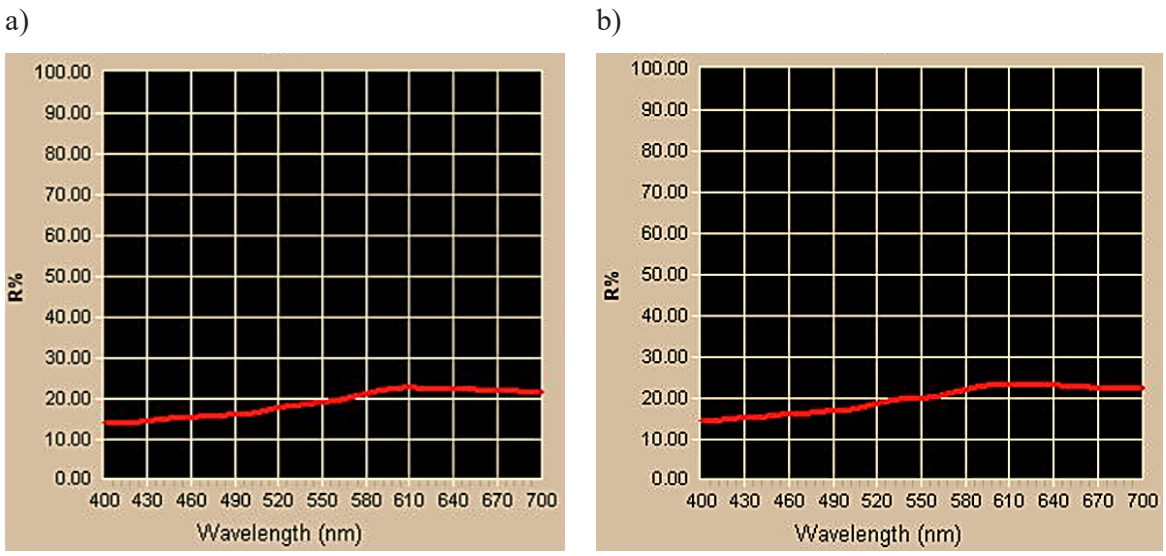

Fig. 8. Remission curves of fabrics: a) B1, b) BP1

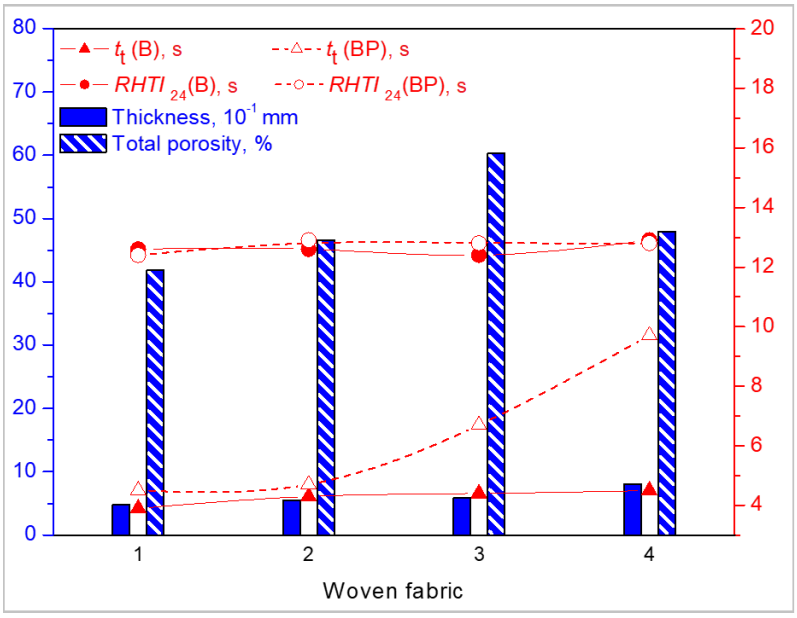

Fig. 9. Dependence of t_t and $RHTI_{24}$ on the porosity and thickness of unmodified and modified basalt fabrics (lines guide the eye)

on the thickness was observed, however, for unmodified fabrics, the t_t increase is milder - 15% (values increase from 3.9 s to 4.5 s), while for modified fabrics the t_t increase is 216% (values increase from 4.5 s to 9.7 s). The biggest difference in the t_t parameter between the modified fabrics and those coated with Parylene C was observed for two fabrics (B3 and B4). This difference may be due to the fact that in the case of fabric B3 (the most porous) and fabric B4 (the thickest, the only one with a different weave from the other three fabrics), Parylene C formed a thicker heat-insulating layer than in the case of fabrics: B1 and B2.

The Parylene C coating was identified on the basalt fabric surfaces (Figure 3). By coating the fabric surface with a thin conformal layer of Parylene C, the fibrous structure was protected against damage (due to fraying). Thanks to the penetrating capacity of the process, each fiber and each node separately were stabilized, resulting in strengthening the stability of the entire structure. The Parylene C coating increased the usability of basalt fabrics, eliminated the effect of skin irritation, and contributed to the creation of skin-friendly material.

5. Conclusions

The following conclusions can be drawn as a result of the research.

– The outcomes of the contact heat method showed the Parylene C coating presence improved the thermal insulation of all composites. In the case of BP3 the threshold time t_t was 6.7 s, while for BP4 it was 9.7 s. It means that the first efficiency level of protection against contact heat was reached.
– The results of the radiant heat method showed that use of the Parylene C coating did not cause changes in thermal insulation against heat radiation of all tested composites in comparison to unmodified basalt fabrics. The radiant heat transfer index $RHTI_{24}$ reached a value in the range of 12.4 s - 12.9 s.
– Micro-CT analysis results proved that the use of Parylene C coating eliminated the effect of skin irritation. The skin-friendly material obtained can provide better sensory comfort of user.

Acknowledgment

These studies were financed from funds assigned from: I42/501-4-42-1-1 statutory activity by Lodz University of Technology. Institute of Material Science of Textiles and Polymer Composites. Poland; the "Innovative Textiles 2020+" no. RPLD.01.01.00-10-0002/17-00 investment project within the Regional Operational Programme for Łódzkie 2014-2020.

Conflicts of Interest

The authors declare no conflict of interest.

References

1. V.P. Kumbhar, An overview: Basalt rock fibers - New construction material, Acta Eng. Int. 2014, Vol. 2, No. 1, p. 11-18.
2. H. Jamshaid, R. Mishra, A green material from rock: Basalt fiber - A review, J. Text. Inst. 2016, Vol. 107, No. 7, p. 923-937.
3. T. Ayub, N. Shafiq, S.U. Khan, Compressive stress-strain behavior of HSFRC reinforced with basalt fibers, J. Mater. Civ. Eng. 2016, Vol. 28, No. 4, 06015014.
4. H. Liu, Y. Yu, Y. Liu, M. Zhang, L. Li, L. Ma, Y. Sun, W. Wang, A Review on basalt fiber composites and their applications in clean energy sector and power grids, Polymers 2022, Vol. 14, No. 12, p. 1-20.
5. A. Chelliah, Mechanical properties and abrasive wear of different weight percentage of TiC filled basalt fabric reinforced epoxy composites, Mater. Res. 2019, Vol. 22, No. 2, e20180431.
6. J. Militký, V. Kovacic, V. Bajzík, Mechanical properties of basalt filaments, Fibers Text. East. Eur. 2007, Vol. 15, No. 5-6, p. 49-53.
7. M.A.A. El-Baky, M.A. Attia, M.M. Abdelhaleem, M.A. Hassan, Flax/basalt/E-glass fibers reinforced epoxy composites with enhanced mechanical properties, Journal of Natural Fibers 2022, Vol. 19, No. 3, p. 954-968.
8. Z. Li, J. Ma, H. Ma, X. Xu, Properties and applications of basalt fiber and its composites, IOP Conf. Ser. Earth Environ. Sci. 2018, Vol. 186, p. 1-7.
9. V. Fiore, T. Scalici, G. Di Bella, A. Valenza, A review on basalt fibre and its composites, Compos. Part B-Eng. 2015, Vol. 74, p. 74-94.
10. G. Song, S. Mandal, R. Rossi (Eds.), Thermal protective clothing for firefighters, Woodhead Publishing Series in Textiles, Elsevier, Amsterdam 2017.
11. Q.Q. Zhou, X.P. Liang, J. Wang, H. Wang, P. Chen, D. Zhang, S.M. Yang, J.X. Li, Preparation of activated aluminum-coated basalt fiber mat for defluoridation from drinking water, J. Sol-Gel Sci. Technol. 2016, Vol. 78, No. 2, p. 331-338.
12. P. Miśkiewicz, I. Frydrych, M. Tokarska, W. Pawlak, Study on some thermal and electrical properties of basalt fabric modified with metal and ceramics as a result of magnetron sputtering, Polymers 2019, Vol. 11, No. 12. p. 1-15.
13. Y. Liu, Y. Yu, H. Du, The influence of two types of functional particles on the electromagnetic properties and mechanical properties of double-layer coated basalt fiber fabrics, Textile Research Journal 2022, Vol. 92, No. 15-16, p. 2591-2604.
14. T. Kolar, V. Kokol, Synergistic effect of screen-printed single-walled carbon nanotubes and phosphorylated cellulose nanofibrils on thermophysiological comfort, thermal/UV resistance, mechanical and electroconductive properties of flame-retardant fabric, Materials (Basel) 2021, Vol. 14, No. 23, p. 1-23.
15. A.K. Puszkarz, W. Machnowski, Simulations of heat transfer through multilayer protective clothing exposed to flame, Autex Res. J. 2022, Vol. 22, No. 3, p. 298-304.
16. M. Renard, A.K. Puszkarz, Modeling of heat transfer through firefighters multilayer protective clothing using the computational fluid dynamics assisted by X-ray microtomography and thermography, Materials 2022, Vol. 15, No. 15, p. 1-17.
17. C. Watson, O. Troynikov, H. Lingard, Design considerations for low-level risk personal protective clothing: a review, Industrial Health 2019, Vol. 57, p. 306-325.
18. J.Y. Xu, Y.C. Sun, X.X. Li, R.X. Chen, Influence of layer configuration on protecting effect of thermal protective clothing containing PCM, In: Silk, Protective Clothing and Eco-Textiles, L. Bai, G.-Q. Chen (Eds.), Trans Tech Publications Ltd, Stafa-Zurich 2013, p. 639-642.

19. K. Wang, C. Fu, A. Xu, M. Wu, L. Jia, W. Xu, B. Su, Z. Xia, Skin-friendly and highly fireproof fabric up to 1142 °C weaved by basalt @ polyimide yarns, Composites Part B: Engineering 2022, Vol. 246, p. 1-9.
20. P. Miśkiewicz, M. Tokarska, I. Frydrych, M. Makówka, Assessment of coating quality obtained on flame-retardant fabrics by a magnetron sputtering method, Materials 2021, Vol. 14, No. 6, p. 1-11.
21. P. Miśkiewicz, I. Frydrych, W. Pawlak, A. Cichocka, Modification of surface of basalt fabric on protecting against high temperatures by the method of magnetron sputtering, Autex Res. J. 2019, Vol. 19, No. 1, p. 36-43.
22. T. Liu, M. Chen, J. Dong, R. Sun, M. Yao, Numerical simulation and experiment verified for heat transfer processes of high-property inorganic fiber woven fabrics, Text. Res. J. 2022, Vol. 92, No. 13-14, p. 2368-2378.
23. R. Hrynyk, I. Frydrych, E. Irzmańska, A. Stefko, Thermal properties of aluminized and non-aluminized basalt fabrics, Text. Res. J. 2013, Vol. 83, No. 17, p. 1860-1872.
24. P. Miśkiewicz, I. Frydrych, M. Makówka, Examination of selected thermal properties of basalt composites, Fibers Text. East. Eur. 2020, Vol. 28, No. 2, p. 103-109.
25. M. Szwarc, Some remarks on the CH_2[graphic omitted]CH_2 molecule, Discuss. Faraday Soc. 1947, Vol. 2, p. 46-49.
26. W.F. Gorham, Para-xylyleny polimers, United States Patent Office No. 3,342,754, Patented September 19, 1967.
27. W.F. Gorham, A new, general synthetic method for the preparation of linear Poly-pxylylenes, Journal of Polymer Science Part A-1: Polymer Chemistry 1966, Vol. 4, No. 12, p. 3027-3039.
28. S. Buchwalder, A. Borzì, J.J. Diaz Leon, F. Bourgeois, C. Nicolier, S. Nicolay, A. Neels, O. Zywitzki, A. Hogg, J. Burger, Thermal analysis of parylene thin films for barrier layer applications, Polymers 2022, Vol. 14, No. 17, p. 1-12.
29. B. Humphrey, Using parylene for medical substrate coating, Medical Plastics and Biomaterials Magazine, January 1996.
30. A. Nosal, A. Zydorczyk, A. Sobczyk-Guzenda, L. Głuchowski, H. Szymanowski, M. Gazicki-Lipman, Parylene coatings on biological specimens, Journal of Achievements in Materials and Manufacturing Engineering 2009, Vol. 37, No. 2, p. 442-447.
31. M. Gazicki-Lipman, Vapor deposition polimerization of para-Xylylene derivatives – Mechanism and applications, Journal of Vacuum Society of Japan 2007, Vol. 50, No. 10, p. 601-608.
32. G.P. Spellman, J.F. Carley, L.A. Lopez, Vacuum deposition of parylene films: Influence of process factors and baffling on film-thickness distribution, Journal of Plastic Film & Sheeting 1999, Vol. 15, No. 4, p. 308-328.
33. T. Marszałek, M. Gazicki-Lipman, J. Ulański, Parylene C as versatile dielectric material for organic field-effect transistors, Beilstein Journal of Nanotechnology 2017, Vol. 8, p. 1532-1545.
34. M. Cieślik, M. Gołda, A. Kotarba, Parylene coating for metal implant surface protection, Engineering of Biomaterials 2012, No. 116-117, p. 39-41.
35. C. Hassle, R.P. von Metzen, P. Ruther, T. Stieglitz, Characterization of Parylene C as an encapsulation material for implanted neural prostheses, J. Biomed. Mater. Res. Part B 2010, Vol. 93, No. 1, p. 266-274.
36. M. Cieślik, K. Engvall, J. Pan, A. Kotarba, Silane–parylene coating for improving corrosion resistance of stainless steel 316L implant material, Corros. Sci. 2011, Vol. 53, No. 1, p. 296-301.
37. M. Kamińska, W. Okrój, W. Szymański, W. Jakubowski, P. Komorowski, A. Nosal, H. Szymanowski, M. Gazicki-Lipman, H. Jerczyńska, Z. Pawłowska, B. Walkowiak, Interaction of Parylene C with biological objects, Acta of Bioengineering and Biomechanics 2009, Vol. 11, No. 3, p. 19-25.
38. B.J. Kim, E. Meng, Micromachining of Parylene C for bioMEMS, Polymers for Advanced Technologies 2016, Vol. 27, No. 5, p. 564-576.
39. A.A. Guermoudi, P.Y. Cresson, A. Ouldabbes, G. Boussatour, T. Lasri, Thermal conductivity and interfacial effect of parylene C thin film using the 3-omega method, J Therm Anal Calorim 2021, Vol. 145, No. 1, p. 1-12.
40. B.G. Halvorson, N. Kerr, Effect of light on the properties of silk fabrics coated with Parylene-C, Studies in Conservation 1994, Vol. 39, No. 1, p. 45-56.
41. P. Miśkiewicz, M. Tokarska, I. Frydrych, A. Nosal, Composite based on basalt fabric intended for protection against burns, especially for the palm side of a protective glove and the method of manufacturing this composite, Patent Application PL, P.445458, July 4, 2023.
42. ISO 12127-1:2015. Clothing for Protection Against Heat and Flame—Determination of Contact Heat Transmission Through Protective Clothing or Constituent Materials—Part 1: Contact Heat Produced by Heating Cylinder.
43. ISO 11612:2015. Protective Clothing—Clothing to Protect Against Heat and Flame—Minimum Performance Requirements.
44. ISO 6942:2022. Protective Clothing—Protection Against Heat and Fire—Method of Test: Evaluation of Materials and Materials Assemblies When Exposed to a Source of Radiant Heat.
45. A.K. Puszkarz, J. Wojciechowski, I. Krucińska, Analysis of the thermal insulation of textiles using thermography and CFD simulation based on micro-CT models, Autex Res. J. 2020, Vol.20, No.3, p.345-351.
46. A.K. Samanta (Ed.), Colorimetry, IntechOpen, London 2022.
47. ISO 11664-4:2008(E)(CIE S 014-4/E:2007). Colorimetry—Part 4: CIE 1976 L*a*b* colour space.
48. G. Sharma, W. Wu, E.N. Dalal, The CIEDE2000 color-difference formula: Implementation notes, supplementary test data, and mathematical observations, COLOR Research and Application 2005, Vol. 30, No. 1, p. 21-30.
49. W.S. Mokrzycki, M. Tatol, Color difference Delta E - A survey, Machine Graphics and Vision 2011, Vol. 20, No. 4, p. 383-411.
50. ISO/IEC Guide 98-3:2008. Uncertainty of Measurement—Part 3: Guide to the Expression of Uncertainty in Measurement (GUM:1995).